EMERGING MINDS
JOURNAL FOR STUDENT RESEARCH

ISSN 2976-9094
EMJSR 2024,Vol 2 (1):69-77
https://doi.org/10.59973/emjsr.113

Received: 2024-07-05
Accepted: 2024-07-10
Published: 2024-07-11

Radio Observations of Tidal Disruption Events Around Direct Collapse Black Holes at Cosmic Dawn

Nathan Herbert[1,*]

[1]University of Portsmouth, School of Mathematics and Physics, Portsmouth, PO1 3FX, United Kingdom

[*]Corresponding author: nathan.herbert90@gmail.com

Abstract - Primordial haloes immersed within intermediate Lyman-Werner (LW) UV backgrounds are theorised to be the seeds of supermassive primordial stars (SMSs) that could be the origin of the first quasars in our universe. Only extreme levels of LW fluxes however will destroy the molecular hydrogen H_2 in these haloes, resulting in much less massive stars in the early stages of our universe. This investigation considers the collapse in haloes within weaker LW background that were much more common in the primordial universe, and allowed for the survival of some H_2 within these haloes. The survival of H_2 along with $T_{vir} \sim 10^4$ K allows the atomic cooling of H_2 to begin, triggering the baryonic collapse within these haloes. These flows are predicted to result in SMSs on the order of a few $\times 10^5$ $M_\odot$ before collapsing to a DCBH due to general relativistic instabilities within their cores. The stars formed through these mechanisms could be the origin seeds of intermediate mass black holes found within dwarf galaxies today, or even create a secondary tier of less massive but still highly luminous quasars at a redshift $z > 7$. Some of these stars form in binaries and small clusters, raising the possibility of future detections of gravitational waves from BH mergers by LISA. This investigation considers the tidal disruption events (TDEs) of lower mass Pop III stars that form within the nuclear accretion disc of these DCBHs, the potential observation of these TDE afterglows in the radio, and the subsequent identification of their host DCBHs. We find that the radio observation of the afterglow of 15 $M_\odot$ and 40 $M_\odot$ TDEs due to 10^4 $M_\odot$ DCBHs would be visible up to z = 20 by SKA and ngVLA.

Keywords - quasars: general ; dark ages ; galaxies: high-redshift ; first stars ; black hole physics ; early universe

1 Introduction

Thousands of quasars have been discovered, with over 300 discovered at $z > 6$ (and 10 at $z > 7$) [1-5] and massive black holes have also been detected at redshift $z \sim 10$ through the JADES and CEERS surveys [6-7] from the James Webb Space Telescope (JWST). Historically, Direct Collapse Black Holes (DCBHs) formed by the General Relativistic Instability (GRI) collapses of supermassive primordial stars in hot-atomically-cooled haloes at $z \sim 15$ - 20 have been thought of as the seeds of these high redshift quasars [8]. They are believed to have formed when the haloes grow to $\sim 10^7$ $M_\odot$and have a virial temperature of $T_{vir} \sim 10^4$ K without having forming stars due to being immersed in strong Lyman-Werner (LW)

UV fluxes which destroys the molecular hydrogen (H_2), which is responsible for atomically cooling gases, preventing fragmentation in lower mass haloes [9-12].
The general relativistic instabilities occur as the pressure within the cores of these SMSs is radiation dominated ($\sim$ 99 %), meaning that they are approaching the Eddington Limit resulting in the cores sitting on the cusp of instability due to the effects of General Relativity (GR). Leading to the smallest of GR corrections being sufficient enough to make the core unstable, resulting in the direct collapse of the core to a DCBH forgoing the supernova process usually associated with the end of the stellar life cycle of SMSs (See [13]).
Atomic cooling due to molecular hydrogen (H_2) is the process in which the stored thermal (kinetic) energy is converted into a form of potential energy upon collisions with other molecules. But H_2 itself is not an efficient coolant as it cannot be induced to emit photons purely through collisions at temperatures of $T_{\rm vir} \sim 10^4$ K. However in the presence of an intermediate LW background, the molecular hydrogen is able to absorb the UV photons, promoting internal electrons into a 'higher' energy, less bound orbit of the molecular atom. This energy gain is then later released in the form of photons with the characteristic energy of the incident LW UV photons. This process on the large scale of primordial haloes allows the cloud of molecular hydrogen to cool down and fragment into clusters as the photons emitted after UV absorption carry energy out of the cloud itself, which is the vital initial part of the complex equation that allows star formation in these early gas haloes (See [14]).
The LW background is a part of the universal background radiation consisting of ultraviolet photons that are able to photo-dissociate molecular hydrogen (H_2) whilst simultaneously not ionising atomic hydrogen (H_1). These UV photons have energies of 11.2 eV - 13.6 eV [15] and is able to photo-dissociate H_2 efficiently through a 2-step process known as the Solomon process [16]. The LW background is a vital aspect to star formation in the early universe as a sufficient flux of LW photons, typically referred to as a strong LW background, can fully disassociate H_2, suppressing star formation within haloes as the essential cooling component no longer remains [17].
But within weak or intermediate LW backgrounds, temperatures of $T_{\rm vir} \sim 10^4$ K start atomic cooling within hydrogen, triggering rapid baryon collapse on the order of $\sim 1 M_\odot$ yr^{-1} at the centre of the halo. Various stellar evolution models predict that these flows result in supermassive primordial stars reaching masses of a few 10^5 $M_\odot$ before collapsing to a DCBH due to GRI within their cores [18-24]. However, recent discoveries have shown that rare, disordered haloes able to form quasars at $z \geq 6$ via strong accretion flows [25-31] formed their own DCBHs irrelevant of UV background, baryon streaming motions or even H_2 atomic cooling [32].
DCBHs are postulated to be the seeds of quasars that are observed across our universe as BHs formed from standard, smaller Pop III are limited to $\sim$ 10 - 1000 $M_\odot$ at birth (e.g.,[33-34]) due to forming in low densities that counteract rapid initial growth [35-39]. DCBHs however can grow at much greater rates if they form in dense, atomically-cooled flows in significantly larger haloes, capable of preserving their fuel supply despite X-ray heating [40]. Rampant stellar collisions within dense, low-metallicity clusters are able to form BHs up to a few thousand $M_\odot$ [41-45], however they may lack the size to become quasars at $z > 7$ [46-48].
The detectability of both DCBHs and SMSs vary greatly. Larger DCBHs, with standard accretions, on the order of $10^4 - 10^5$ $M_\odot$, are able to be detected by JWST up to $z \sim 20$ [49], with SMSs, of up to a few 10^5 $M_\odot$, detections being limited to $z \leq 20$ through JWST, or $z \sim 10 - 12$ through modest gravitational lensing and the Roman Space Telescope (RST) [50].
DCBHs can also be flagged in surveys by strong He II 1640 $\mathring{A}$ emission lines and a lack of metal emission lines [51]. However, the existence of tidal disruption events (TDEs) prove to be a useful tool for astrophysicists, as they not only allow for the possibility of the detection of previously undetected DCBHs due to their extremely bright nature, but they can be highly important in pushing further understanding on how black holes gravitationally influence their environments. We propose that TDEs due to stars formed within the nuclear accretion disc of a DCBH could very well have occurred, and these TDEs would have radio afterglows

significantly brighter than those associated with TDEs that occur today.
The basics of TDE dynamics have been understood for a while due to the works of [52] and [53], laying the foundational model predicting the fluxes of the afterglows produced by a stellar mass TDE due to supermassive black holes. In the case of DCBHs, TDEs occur when a star is tidally disrupted by the central BH. This process starts when the tidal forces exerted upon the star due to the DCBH exceed that of the gravity of the star itself, resulting in the star being torn apart. Assuming a mass M_* and radius R_* for the star, this imbalance of forces occurs at a critical distance of $R_t \sim R_*(M_{BH}/M_*)$ from the DCBH [54]. Most of the matter would be consumed by the black hole, but some the remaining matter is ejected at relativistic velocities. These ejected jets collide with ambient gas surrounding the black hole, resulting in extreme temperatures which begin the emission of synchrotron radiation. This synchrotron radiation is what is observed, known as a radio afterglow. These luminous radio afterglow, that could have a luminosity of $L_{jet} \geq 10^{50}$erg s^{-1}, would last a few years at most [55]. The infalling stars were assumed to have formed within the nuclear accretion disc of a host DCBH due to a H_2-free gas cloud collapsing isothermally due to hydrogen cooling within an atomically cooled primordial halo on the order of $\sim 10^7 - 10^8$ $M_\odot$ [56].
These highly transient events allow for the detection of DCBHs in the radio. [56] found that TDEs due to 10^5 $M_\odot$ DCBHs could be observed at $z \sim 20$ by the Square Kilometer Array (SKA) and next-generation Very Large Array (ngVLA). However, it is now thought that most DCBHs are closer to 10^4 $M_\odot$ because the LW backgrounds required to create them are weaker, and more common. No calculations of radio fluxes from TDEs of these less massive DCBHs have been shown before. Here, we estimate TDE radio fluxes for DCBHs due to 10^4 $M_\odot$ DCBHs at high redshifts and discuss their detectability with respect to current observational techniques and apparatus.
This report is organised as follows. In section 2, we detail the analytical methods carried out to estimate the fluxes that would be observed from a TDE due to a 15 $M_\odot$ and a 40 $M_\odot$ infalling star onto a 10^4 $M_\odot$ DCBHs up to redshift 20. In section 3, we summarise the results obtained from the investigation and shows that radio observations of TDE afterglows may be a feasible option to identify DCBHs at high redshifts. In section 4, we consider the limitations of our models and discuss the next steps of the investigation as we progress with this avenue of research. Section 5 summarises the paper.

2 Numerical Methods

[56] gives a detailed analytical calculation for the formulation of a nuclear cluster around DCBHs and their TDEs. They derive formulations for the fragmentation of the nuclear accretion disc around DCBHs and formation of massive Pop III stars. In this study, we solely focus their 2 equations describing the properties of TDE afterglows. Here, we estimate the peak frequency and the flux of the peak frequency of radio afterglows due to 15 $M_\odot$ and 40 $M_\odot$ TDEs, and apply it across a redshift range of $10 \leq z \leq 20$.

The kinetic energy of the afterglow emission jet can be comparable to or even larger than the binding energy of the seed halo, so TDEs in collapsing atomically cooled haloes will give mechanical feedback. The synchrotron emission from the decelerating jet, specifically in the radio bands, could possibly be detectable at $z \sim 20$.
The characteristic synchrotron frequency within the observers reference frame is:

$$\begin{aligned} \nu_{\max} &= \frac{\Gamma \gamma_{e,m}^2 qB}{2\pi m_e c(1+z)} \\ &\sim 230\text{GHz}\left(\frac{1+z}{11}\right)^{-1} \epsilon_{e,-1}^2 \epsilon_{B,-2}^{1/2} f_{b,-2} E_{j,55} \Gamma_{1.3}^6 \dot{M}_{w,-2}^{3/2} \nu_{w,10}^{-3/2} \end{aligned} \tag{1}$$

where ϵ_e is the acceleration efficiency of the electrons, f_b is the beaming factor of the jet and E_j is the kinetic energy of the jet in $2.4 \times 10^{55}(M_*/40\ M_\odot)$ ergs, where M_* is the mass of the

infalling star.

And hence the corresponding peak flux can be estimated by:

$$\begin{aligned} F_{\nu,\max} &\approx \frac{\sigma_{\rm T} m_{\rm e} c^2 \dot{M}_{\rm w} B \Gamma r_{\rm dec}(1+z)}{12\pi q m_{\rm p} \nu_{\rm w} D_{\rm L}^{-2}} \\ &\sim 360\mu{\rm Jy}\left(\frac{1+z}{11}\right) D_{\rm L,29.5}^{-2} \epsilon_{\rm B,-2}^{1/2} \Gamma_{1.3}^{2} \dot{M}_{\rm w,-2}^{3/2} \nu_{\rm w,10}^{-3/2} \end{aligned} \tag{2}$$

where D_L is the luminosity distance in $10^{29.5}$cm, as a function of redshift, to the source. ϵ_B is the magnetic field amplification efficiency, Γ is the Lorentz factor of the jet in Log_{20} and $\dot{M}$ is the gas accretion rate onto the central BH in $10^{-2}\mathrm{M}_\odot$ yr^{-1}.

But in the case that $\nu \leq \nu_m$, then we just assume $F_{\nu,\max} \propto \nu^{\alpha}$. And here is where we make a series of assumptions in order to simplify (1) and (2), we assume $\dot{M} = 10^{-2}$ $\mathrm{M}_\odot$ yr^{-1} and $\nu_{\rm w} = 10^{10}$cm s^{-1} as fiducial, meaning that 10% of the accreted matter is ejected from the slim disc with $\mathrm{v_{esc}}$ at the innermost regions [56].

Given the assumptions imposed on (1) and (2), as well as further cancellations made, the prescribed magnitudes of the variables allow them to cancel down to approximately 1, this leaves the simplified peak flux and synchrotron frequency equation:

$$\nu_{\max} \sim 230{\rm GHz}\left(\frac{1+z}{11}\right)^{-1} E_{\rm j,55} \tag{3}$$

$$F_{\nu,\max} \sim 360\mu{\rm Jy}\left(\frac{1+z}{11}\right) D_{\rm L,29.5}^{-2} \tag{4}$$

NOTE: $\mathrm{D_L}$ here is found by using a cosmological calculator created by [57] and was initialised using the second-year *Planck* cosmological parameters: $\Omega_{\rm M} = 0.3111 \pm 0.0056$, $\Omega_\Lambda = 0.6889 \pm 0.0056$ and $\mathrm{H_0} = 67.66 \pm 0.42$ [58]. $\mathrm{D_L}$ is given in units of 10^{29}cm by the calculator, so manual conversions were carries out in order to get them to the magnitudes required for (4). These conversions can be seen in Table 1.

But these equations alone do not allow for meaningful conclusions to be drawn from them, as peak frequency and peak flux are not what SKA and ngVLA would observe. The observable fluxes need to be split into the separate detector bands to do this. This involves deriving the flux and frequency at the point of origin. We can estimate the fluxes that would fall into the detector bands of SKA and ngVLA by blueshifting the detector band to the redshift in question, and interpolating the detector band flux by assuming a non-thermal power law spectrum. We assume a non-thermal power law spectrum as the radiation that would be observed from the afterglow of a TDE is not thermal in nature, meaning it is not black body. Instead, the observed flux comes from the synchrotron radiation being emitted by the relativistic charged particles within the afterglow.

We blueshift the detector band across our desired redshift range with the following:

$$\nu_{\rm z} = (1+z)\nu \tag{5}$$

NOTE: ν here is the SKA and ngVLA detector bands being blueshifted (i.e: 500MHz, 1.5GHz, 6.5GHz and 12.5GHz).

And we interpolate the detector band flux assuming the following:

$$F_{\rm z} = \left(\frac{\nu_{\rm z}}{\nu_{\max}}\right)^{\alpha} F_{\nu,\max} \tag{6}$$

NOTE: $F_{\nu,\max}$ here is the flux of the peak frequency for a given redshift as estimated by (2), and $\nu_{\max}$ is the peak frequency for a given redshift as estimated by (1).

Here, flux is assumed to follow a power law in alpha, with alpha denoted as (1/3). In the instances where the blueshifted synchrotron frequency of a specific radio band exceeds the maximum synchrotron frequency from (3) at a certain redshift ($\nu_z > \nu_{\max,z}$), a flux for a TDE cannot be determined for that redshift and further redshifts, essentially cutting the limits of observations to $z - 1$ in that specific radio band due to the lack of models able to predict fluxes in those cases. This important to understand as it informs researchers as to the limits of observation for specific detector bands.

3 Results

The results were obtained by compiling a python code to estimate the flux of a TDE due to a 10^4 $M_\odot$ DCBH in the 500 MHz, 1.5 GHz, 6.5 GHZ and 12.5 GHz detector bands of SKA and ngVLA. A simple 'for' loop was constructed in order to iterate through our redshift array ($10 \leq z \leq 20$), inserting the given values into (3) and (4) as well as the corresponding values for $E_{j,55}$ and $D_{L,29.5}$ to obtain the results seen in Figure 1 and 2. The same was done for (5) and (6) to interpolate the detector band fluxes as seen in Figure 3. The NumPy package was used optimise the performance and efficiency of our numerical operations, and Pandas was used for its ability to untangle data and operate with text files efficiently. Mpatches and Mlines were also employed here to enhance the readability of the final results obtained due to their cluttered nature. Mpatches separates out all the separate frequency bands being operated in into visible groups, whilst Mlines makes the identification between the two infall star mass cases easily distinguishable from each other.

Redshift	D_L(Mpc)	D_L(cm)	$D_{L,29.5}$(cm)
10	106188.0	3.276621878e29	1.03615881
11	118315.9	3.650850063e29	1.15450018
12	130540.7	4.028068272e29	1.27378705
13	142851.2	4.407930908e29	1.39391017
14	155238.5	4.790162247e29	1.51478268
15	167694.7	5.174521819e29	1.63632747
16	180213.6	5.560815012e29	1.75848414
17	192789.6	5.948870129e29	1.88119791
18	205418.0	6.338542142e29	2.00442302
19	218094.6	6.729701453e29	2.12811846
20	230816.0	7.122243149e29	2.25225104

Table 1: Luminosity Distance Conversions calculated using the cosmological calculator (see [57])

Table 1 shows the values obtained from the cosmological calculator, and their conversions to the prescribed magnitudes required for (2). These values were obtained using the cosmological calculator mentioned previously and initialised with the second-year *Planck* cosmological parameters of $\Omega_M = 0.308$, $\Omega_\Lambda = 0.691$ and $H_0 = 67.4$ [58]. This however only output D_L with a magnitude of 10^{29}cm, so additional conversions were needed to get all the values to the required order of $10^{29.5}$cm required for (2).

Figure 1 and 2 show both the peak afterglow flux and peak synchrotron frequency, for both a 15 $M_\odot$ and a 40 $M_\odot$ infalling star. These are both the maximum values as described by (1) and (2). The blue curve indicates the peak frequency and so should be read against the blue axes, therefore the red curve indicates the peak flux and so should be read against the red

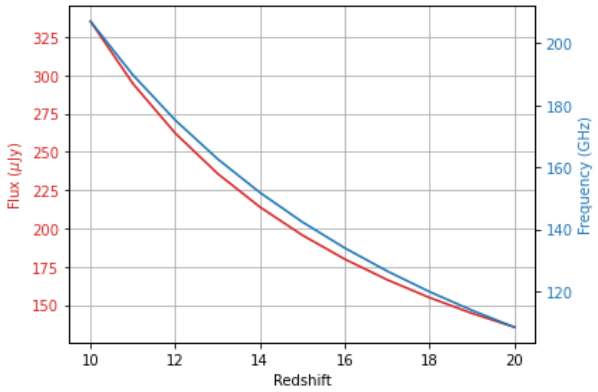

Figure 1: Afterglow Flux and Synchrotron Frequency-Redshift Relation for a 15$M_\odot$ infalling star onto a DCBH

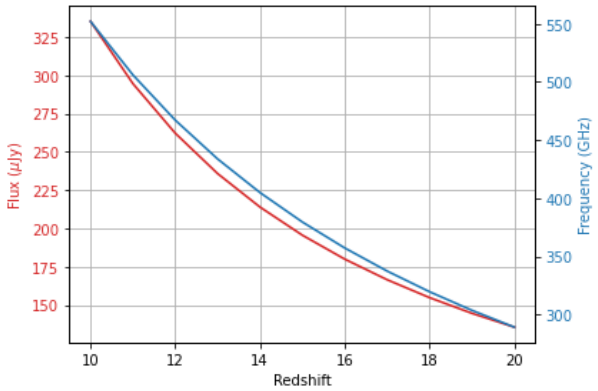

Figure 2: Afterglow Flux and Synchrotron Frequency-Redshift Relation for a 40$M_\odot$ infalling star onto a DCBH

axes. These data sets follow the expected trends for flux profiles as redshift increases. It can be seen that flux is consistent for both 15 $M_\odot$ and 40 $M_\odot$ TDEs, this is due to (2) having no dependency on the kinetic energy of the jet, E_j. Whereas the frequency of the synchrotron radiation increases for the 40 $M_\odot$ TDE, as (1) is dependant upon E_j and is proportional to ($M_*/40M_\odot$). However these figures have little importance when trying to draw conclusions as to the detectability of TDEs, as the peak frequencies here are much larger than the detector bands for both SKA and ngVLA, as these frequencies are not within the observer frame. But they rather serve as a comparison point against (5) as to whether a radio-flux could be observed at a given redshift.

By executing the necessary calculations as described by (5) and (6), the interpolated observer frame fluxes for both a 15 $M_\odot$ and 40 $M_\odot$ TDEs as a function of redshift, as seen in Figure 3, are obtained.

	500MHz	1.5GHz	6.5GHz	12.6GHz
1 hr	4400	2000	1300	1200
10 hr	1391	632	411	379
100 hr	440	200	130	120
1 hr	—	382	220	220
10 hr	—	121	70	70
100 hr	—	38	22	22

Table 2: Top three rows: The sensitivity limits of SKA for 500MHz, 1.5GHz, 6.5GHz and 12.5GHz. Bottom three rows: The same but for ngVLA. The values are in nJy/beam for 1 hr, 10 hr and 100 hr exposure time. (See Table 3 in [59])

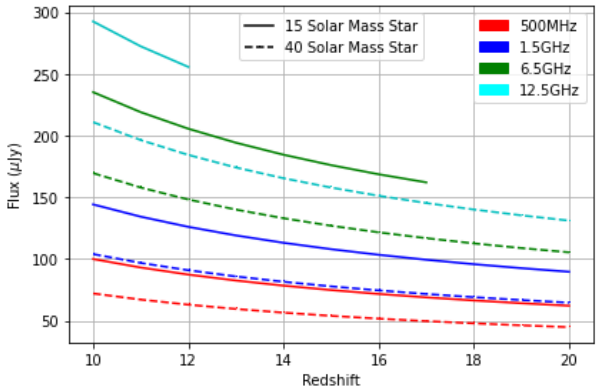

Figure 3: Radio Band isolated Afterglow Flux-Redshift Relation

Table 2 shows all the sensitivity limits for both the SKA and ngVLA, prescribing the minimum fluxes required, in each given frequency band, for an observation to be feasible across a given exposure time. The SKA root mean square (rms) and the ngVLA 5σ rms sensitivity limits for each frequency band are listed in Table 3 of [59]. SKA, a combination of SKA1-Low and SKA1-Mid with a baseline of up to 150 km, will allow for coverage of frequencies of 350 MHz - 24 GHz. And ngVLAs combination of its main interferometric array, Short Baseline Array (SBA) and its Long Baseline Array (LBA) providing a baseline of $\sim$ 8900 km will allow for coverage of $\sim$ 1.2 GHz - 116 GHz.

The cut-offs for 12.5GHz and 6.5GHz lines for a 15 $M_\odot$ TDE occur due to the blueshifted detector frequency exceeding the peak frequency at redshift 13 for the 12.5GHz band, and 18 for the 6.5GHz band. This indicates that no TDE radio fluxes can be observed past redshift 12 in the 12.5GHz detector band, and past redshift 17 in the 6.5GHz detector band for a TDE due to a 15 $M_\odot$ infalling star as we do not have any models that can reliably estimate TDE fluxes given the conditions predicted by the model we use here. Note that the highest fluxes occur at the higher frequencies, but even the lower frequencies have flux values that well exceed the highest detection limits as shown in Table 2, that being the 1 hour exposure time for the 500MHz band of SKA. The lack of comparative detection limits on the plot is attributed to the fact that the magnitude of the fluxes are sufficient enough to surpass all of the detection limits for both SKA and ngVLA for all 1hr, 10hr and 100hr exposure time by a large margin, with a majority of the flux values sitting at $> 10^2 \mu$Jy whereas the detection limits are all limited to $\sim 10^0 \mu$Jy and below. This therefore implies that 40 $M_\odot$ TDEs (in all detector bands), and 15 $M_\odot$ TDEs (in the 500MHz and 1.5GHz detector bands) would be visible to telescopes such as the SKA and ngVLA up to redshifts of 20, or approximately 180 Myr after the Big Bang with only as little as an hour of exposure time.

4 Discussion

Moving forward, next steps will involve starting to estimate TDE rates. This will be done by first estimating the number density of DCBHs per cubic Mpc for any given redshift, which will depend upon the number density in intermediate Lyman-Werner backgrounds per cubic Mpc for any given redshift as the presence of a strong Lyman-Werner UV background will result in the complete suppression of star formation within primordial haloes. We must also estimate the number density of DCBHs that are actively destroying stars in TDEs per cubic Mpc for any given redshift, as not all TDEs will result in an afterglow visible in the radio. This will allow us to estimate the likelihood of making a radio observation of a TDE dependant upon observation time and redshift being observed. This in conjunction with our flux estimates becomes vital to know when submitting proposals for telescope time, as it is essential to show both that the targets produced fluxes are within the frequency range

and have sufficient fluxes to be detected by the telescope, and the likelihood of detecting said target within a given time allocation of telescope time is reasonable. So by obtaining the estimated TDE rates, we can progress this study to an observational phase potentially as early as as 2028 with the beginning of the PI proposals for SKA.

The decision to adopt $15M_\odot$ and $40\ M_\odot$ for the infalling stars was based upon the mechanisms of Pop III star formation in the early universe. Stars forming only from H and He are thought to have characteristic masses of a few $\times 10\ M_\odot$ - $100\ M_\odot$. [34 & 60] also find that main sequence Pop III stars have a typical mass range of a few $\times 10\ M_\odot$ - $100\ M_\odot$ with those having masses of several $\times 10\ M_\odot$ being more common. This discovery is based upon simulations of the Initial Mass Function (IMF) of Pop III in the early universe, which describes the initial mass distribution of a population of stars during star formation. [32] carried out simulations of the IMF of Pop III stars in primordial haloes, finding that typical stellar mass range to be $0.1\ M_\odot - 40\ M_\odot$, with 55 stars having masses $> 20\ M_\odot$ and seven having masses of $10\ M_\odot - 20\ M_\odot$. This implies that the results obtained by carrying out estimates of TDE fluxes due to $15\ M_\odot$ and $40\ M_\odot$ stars being tidally destroyed by $10^4\ M_\odot$ DCBHs will be more what is expected upon possible observations within future radio surveys.

The limitations of this investigation sit within the increments of the chosen redshift range being operated in. The results could be further optimised and enhanced by choosing to run these estimates with an increment of z = 0.1 or even z = 0.01 as opposed to the z = 1 increment used here. This would boost the accuracy as to the exact redshifts observations would be cut off within specific detector bands for both SKA and ngVLA. This could be further built upon by extending the range of redshifts covered, i.e: past z = 20, as to ascertain the theoretical limits of detection with respect to the redshift of the origin TDE as our model here predicts fluxes to be sufficient enough for detection at redshifts exceeding $z = 20$.

The absence of the effect of cosmic dust within our model stems from simple laws of physics. Given the wavelengths of radiation we are operating with (0.024m - 0.6m), cosmic dust has a negligible to no effect at all on the fluxes we predict to observe as at those wavelengths, as the radiation would penetrate fully through any cosmic dust that it may come across, as cosmic dust is generally ¿ 0.1 mm in diameter. However, that is not the only reasoning behind our decision to omit the effect of cosmic dust. Cosmic dust is believed to have formed anywhere from 4-7 billion years ago, but more recently, [61] may have found some of the earliest occurrences of cosmic dust in our universe, dating back to $z \sim 8$, or ~ 600 Myr after the big bang. But given that discovery, the regime of redshifts we are working within exceed that of even the earliest existence of cosmic dust.

As SKA and ngVLA are powerful radio telescopes, they are optimised for probing high redshift cosmological events as the origin optical or even UV spectra will be shifted to within the radio which is the range in which SKA and ngVLA are optimised for surveying, allowing for the direct observation of these high redshift events. Using SKA and ngVLA to search for these high redshift radio-fluxes due to TDEs of $10^4\ M_\odot$ may be the only way DCBHs can be directly detected at cosmic dawn for the foreseeable future.

Furthermore, due to the estimated radio-fluxes being sufficient enough, it is also possible that they could also be detectable by VLA and LOFAR (the Low Frequency Array) up to redshift 20. In fact, its possible that they could have already detected these events, and these detections would exist today within the VLA and LOFAR legacy data bases. This would require a machine learning algorithm to search through the enormous amount of data within those archives to look for high redshift transients. This would give researchers years worth of observational data to search through looking for evidence of TDEs occurring at high redshifts whilst simultaneously searching in the present via SKA and ngVLA.

However, the search for TDE afterglows due to $10^4\ M_\odot$ DCBHs at cosmic dawn will not truly begin until after the construction of SKA and ngVLA is complete. With SKA proposed to complete construction in 2030 and ngVLA proposed to complete in 2029, full scientific operation of SKA will not begin until 2026 with their large scale Key Science Projects (KSP) proposals (See [62]) and ngVLA initiate early science proposals beginning in 2031 with

full scientific capabilities projected to launch in 2037 (See [63]). This means that it may be possible to observe the TDE afterglows due to DCBHs as early as 2026. However, given that our models predict that it may be possible to observe TDE afterglows due to 10^4 $M_\odot$ DCBHs with as little as an hour of exposure time, this investigation is more suited to the PI proposals for SKA as it would not require multiple observational cycles to obtain the data required which is the baseline for the KSP proposals. The PI proposals are projected to begin in early 2028.

But we cannot ignore the potential benefits this investigation poses to the scientific community as a whole, as the direct detection of DCBHs at cosmic dawn may help to further understand of the formation mechanisms and evolution paths of black holes, particularly supermassive black holes observed within galactic nuclei as this still remains a mystery. It could also serve as a catalyst for advancements in our understanding of dark matter and dark energy physics by providing indirect evidence of the distribution and behaviour of dark matter and energy in the primordial universe. This may also help in gaining insight into our cosmic structure as a whole, both it's evolution and the formation of large scale structures. However it's not just the scientific community that benefits from theoretical endeavours, society sees the trickle down effect from the pursuits of turning theory into reality in the form of technology. The pursuit of understanding the origins of DCBHs requires technological marvels, leading to advancements in observational instruments, such as SKA and ngVLA, and data analysis techniques which often have broader applications than just the primordial universe or even astrophysics as a whole.

5 Conclusion

The presence of a hybrid Lyα/H_2 cooling mechanism results in the formation of a phased medium within primordial haloes, giving rise to supermassive primordial stars of a few 10^3 $M_\odot$ - 10^6 $M_\odot$ at birth. These stars could potentially serve as the seeds for luminous quasars observed at $z > 7$.

Some of these stars formed in binaries or clusters, raising the possibility of future detections of gravitational waves from BH mergers from GW observatories such as LIGO/LISA. Extending to the detectability of these stars and their potential identification through phenomena such as TDEs. Specifically, this study focused on estimating radio fluxes from TDEs associated with 10^4 $M_\odot$ DCBHs at high redshifts, providing a model predicting the observable peak flux of TDEs across a redshift range of $10 \leq z \leq 20$. The conclusions of this investigation are summarised below:

- Observations of 15 $M_\odot$ TDEs in the 12.5 GHz and 6.5 GHz detector bands are limited to z = 12 and z = 17 respectively.
- Remaining TDE flux estimates for 15 $M_\odot$ (in the 500 MHz and 1.5 GHz detector bands) and 40 $M_\odot$ in all detector bands TDEs are NOT limited, and are predicted to be visible up to z = 20 by both SKA and ngVLA.
- The estimated fluxes in all detector bands for both 15 $M_\odot$ and 40 $M_\odot$ TDEs exceed even the highest detection limits of SKA and ngVLA, indicating that TDEs due to 10^4 $M_\odot$ DCBHs would be visible up to z = 20 with only 1 hour of exposure time.
- Our predicted fluxes are sufficient enough that its feasible to detect TDE afterglows due to 10^4 $M_\odot$ DCBHs past $z = 20$, but further modelling is required to determine the limit of detectability of these events.

The results suggested that given the capabilities of instruments like SKA, ngVLA and advancements in radio observations, the detection of TDEs and subsequent identification of their host DCBHs at high redshifts may become feasible. This leads the the potential to further our understanding of our universe as we approach cosmic dawn through the indirect

evidence obtained by this study. But detailed observational work will need to be carried out in order to test the validity of the conclusions drawn here.

In summary, the investigation offers insights into the formation mechanisms of early stars, the potential origins of quasars, and the prospects for detecting these phenomena.

Acknowledgements

This paper is based on the research done in my final year masters project, and I would like to thank my supervisor, Daniel Whalen, for his support and guidance throughout.

References

[1] Mortlock D. J., et al., 2011, Nature, 474, 616

[2] Matsuoka Y., et al., 2019, ApJ, 872, L2

[3] Yang J., et al., 2020, ApJ, 897, L14

[4] Wang F., et al., 2021, ApJ, 907, L1

[5] Fan X., Ba nados E., Simcoe R. A., 2023, ARAA, 61, 373

[6] Bogdan A., et al., 2023, doi:10.48550/arXiv.2305.15458, p. arXiv:2305.15458

[7] Maiolino R., et al., 2023, arXiv e-prints, p. arXiv:2305.12492

[8] Chandrasekhar S., 1964, ApJ, 140, 417

[9] Yue B., Ferrara A., Salvaterra R., Xu Y., Chen X., 2014, MNRAS, 440, 1263

[10] Dijkstra M., Ferrara A., Mesinger A., 2014, MNRAS, 442, 2036

[11] Agarwal B., Smith B., Glover S., Natarajan P., Khochfar S., 2016, MNRAS, 459, 4209

[12] Latif M. A., Bovino S., Grassi T., Schleicher D. R. G., Spaans M., 2015, MNRAS, 446, 3163

[13] Haemmerl Al' L., 2021, Astronomy amp; Astrophysics, 650, A204

[14] Becerra F., Greif T. H., Springel V., Hernquist L. E., 2014, Monthly Notices of the Royal Astronomical Society, 446, 2380ˆa A S2393

[15] Incatasciato A., Khochfar S., O A sorbe J., 2023, Monthly Notices of the Royal Astronomical Society, 522, 330

[16] Spinoso D., Bonoli S., Valiante R., Schneider R., Izquierdo-Villalba D., 2022, Monthly Notices of the Royal Astronomical Society, 518, 4672

[17] Regan J. A., Downes T. P., 2018, Monthly Notices of the Royal Astronomical Society, 478, 5037ˆa A S5049

[18] Hosokawa T., Yorke H. W., Inayoshi K., Omukai K., Yoshida N., 2013, ApJ, 778, 178

[19] Umeda H., Hosokawa T., Omukai K., Yoshida N., 2016, ApJ, 830, L34

[20] Woods T. E., Heger A., Whalen D. J., Haemmerl e L., Klessen R. S., 2017, ApJ, 842, L6

[21] Haemmerl e L., Woods T. E., Klessen R. S., Heger A., Whalen D. J., 2018, MNRAS, 474, 2757

[22] Woods T. E., Patrick S., Whalen D. J., Heger A., 2021a, arXiv e-prints, p. arXiv:2112.09142

[23] Woods T. E., Patrick S., Elford J. S., Whalen D. J., Heger A., 2021b, ApJ, 915, 110

[24] Herrington N. P., Whalen D. J., Woods T. E., 2023, MNRAS, 521, 463

[25] Di Matteo T., Khandai N., DeGraf C., Feng Y., Croft R. A. C., Lopez J., Springel V., 2012, ApJ, 745, L29

[26] Di Matteo T., Croft R. A. C., Feng Y., Waters D., Wilkins S., 2017, MNRAS, 467, 4243

[27] Huang K.-W., Di Matteo T., Bhowmick A. K., Feng Y., Ma C.-P., 2018, MNRAS, 478, 5063

[28] Tenneti A., Di Matteo T., Croft R., Garcia T., Feng Y., 2018, MNRAS, 474, 597

[29] Spinoso D., Bonoli S., Valiante R., Schneider R., Izquierdo-Villalba D., 2022, Monthly

[30] Valentini M., Gallerani S., Ferrara A., 2021, MNRAS, 507, 1

[31] Lupi A., Haiman Z., Volonteri M., 2021, MNRAS, 503, 5046

[32] Latif M. A., Whalen D. J., Khochfar S., Herrington N. P., Woods T. E., 2022a, Nature, 607, 48

[33] Hirano S., Hosokawa T., Yoshida N., Umeda H., Omukai K., Chi- aki G., Yorke H. W., 2014, ApJ, 781, 60

[34] Hirano S., Hosokawa T., Yoshida N., Omukai K., Yorke H. W., 2015, MNRAS, 448, 568

[35] Whalen D., Abel T., Norman M. L., 2004, ApJ, 610, 14

[36] Kitayama T., Yoshida N., Susa H., Umemura M., 2004, ApJ, 613, 631

[37] Alvarez M. A., Wise J. H., Abel T., 2009, ApJ, 701, L133

[38] Whalen D. J., Fryer C. L., 2012, ApJ, 756, L19

[39] Smith B. D., Regan J. A., Downes T. P., Norman M. L., O'Shea B. W., Wise J. H., 2018, MNRAS, 480, 3762

[40] Johnson J. L., Whalen D. J., Li H., Holz D. E., 2013, ApJ, 771, 116

[41] Devecchi B., Volonteri M., 2009, ApJ, 694, 302

[42] Latif M. A., Omukai K., Habouzit M., Schleicher D. R. G., Volon- teri M., 2016, ApJ, 823, 40

[43] Sakurai Y., Yoshida N., Fujii M. S., Hirano S., 2017, MNRAS, 472, 1677

[44] Reinoso B., Schleicher D. R. G., Fellhauer M., Klessen R. S., Boekholt T. C. N., 2018, AA, 614, A14

[45] Boekholt T. C. N., Schleicher D. R. G., Fellhauer M., Klessen R. S., Reinoso B., Stutz A. M., Haemmerl e L., 2018, MNRAS, 476, 366

[46] Smidt J., Whalen D. J., Johnson J. L., Surace M., Li H., 2018, ApJ, 865, 126

[47] Latif M. A., Khochfar S., 2020, MNRAS, 497, 3761

[48] Zhu Q., Li Y., Li Y., Maji M., Yajima H., Schneider R., Hernquist L., 2022, MNRAS, 514, 5583

[49] Whalen D. J., Surace M., Bernhardt C., Zackrisson E., Pacucci F., Ziegler B., Hirschmann M., 2020, ApJ, 897, L16

[50] Surace M., et al., 2018, ApJ, 869, L39

[51] Wang L., et al., 2017, arXiv:1710.07005

[52] Rees M. J., 1988, Nature, 333, 523

[53] Evans C. R., Kochanek C. S., 1989, ApJ, 346, L13

[54] Hills J. G., 1975, Nature, 254, 295

[55] Reg os E., Vink o J., Stermeczky Z. V., 2021, ApJ, 909, 64

[56] Kashiyama K., Inayoshi K., 2016, ApJ, 826, 80

[57] Wright E. L., 2006, PASP, 118, 1711

[58] Planck Collaboration et al., 2020, AA, 641, A6

[59] Latif M. A., Aftab A., Whalen D. J., 2024, arXiv e-prints, p. arXiv:2401.07910

[60] Hirschmann M., Dolag K., Saro A., Bachmann L., Borgani S., Burkert A., 2014, MNRAS, 442, 2304

[61] Witstok J., et al., 2023, Nature, 621, 267

[62] Observatory S., 2024, Scientific Timeline — SKAO, https://www. skao.int/en/science-users/159/scientific-timeline

[63] ngVLA 2024, Project Timeline, https://ngvla.nrao.edu/